Modeling of a Fluidized Bed Propylene Polymerization Reactor Operated in Condensed Mode

Ranjeet P. Utikar,[1,2] Yogesh M. Harshe,[2] Anurag Mehra,[1] Vivek V. Ranade[2]

[1]*Department of Chemical Engineering, Indian Institute of Technology Bombay, Powai, India*
[2]*Industrial Flow Modeling Group, National Chemical Laboratory, Pune 411008, India*

Received 22 December 2006; accepted 16 October 2007
DOI 10.1002/app.27748
Published online 4 February 2008 in Wiley InterScience (www.interscience.wiley.com).

ABSTRACT: The gas-phase polymerization of propylene is one of the most widely accepted and commercially used processes for the manufacture of polypropylene (PP). Because of the highly exothermic nature of polymerization reactions, temperature runaway and subsequent polymer melting and agglomeration may occur, and the reactor has to be operated in a small operating window for safety. The addition of liquid monomer for heat removal (condensed mode) broadens the operating window and can substantially increase (by 50–100%) the capacity of given reactor hardware. This article describes the extension of a comprehensive mathematical model for the simulation of fluidized bed PP reactors to include the condensed mode of operations. The model is used to determine the influence of the operating parameters on the polymer properties and particle size distribution. The model is also used to determine the effects of two active sites and the reaction kinetics on macroscopic variables. The developed framework is useful for simulating multimonomer, multisite Ziegler–Natta-type olefin fluidized bed polymerization reactors operated under condensed mode. © 2008 Wiley Periodicals, Inc. J Appl Polym Sci 108: 2067–2076, 2008

Key words: modeling; polyolefins; Ziegler–Natta polymerization

INTRODUCTION

The gas-phase propylene polymerization in a fluidized bed is one of the most widely accepted and commercially used processes for the manufacture of polypropylene (PP). In this process, small catalyst particles (20–80 μm) react with the incoming fluidizing gas (monomer) to form a broad distribution (100–5000 μm) of polymer particles.[1] In these reactors, the monomer conversion is limited by the rate at which the heat of polymerization can be removed from the reactor.

The heat of polymerization is removed as sensible heat by circulation of the hot recycled gas stream from the reactor through the compressor and heat exchanger and back into the reactor after it is mixed with fresh feed. At the same time, the gas flow rate is limited to prevent the excessive entrainment of solids. As a result, the productivity of these reactors is severely limited by their heat removal capacity. To increase the capacity, liquid propylene is added (condensed mode). The injected liquid evaporates by coming in contact with hot solids. This broadens the operating window and can substantially increase (by 50–100%) the capacity of given reactor hardware.[2] The success of this technology lies in the proper design of the liquid injection system. Improper design of the system may lead to various undesirable scenarios such as local hot/cold spot formation, agglomeration of polymer particles, and defluidization of the bed. Models based on first principles relate the operating and design parameters to the performance of the reactor and offer insight into these issues.

Several researchers have contributed to the development of polyolefin fluidized bed reactor (FBR) models. The models developed so far have focused on either of the two major aspects of fluidized bed PP reactors, namely, product properties and reactor performance or particle size distribution (PSD). For the prediction of product properties and reactor performance, steady state[3,4] and dynamic[5,6] models have been proposed. Recently, we[7] presented a model that simultaneously predicts both polymer properties and PSD. The generalized framework of a dynamic model based on the mixing cell approach and detailed polymerization kinetics coupled with a population balance model for PSD was developed. A user-friendly computer program called Polyolefin Reactor Simulator (PoRE), which implements the mathematical model, was developed. Rigorous multimonomer, multisite polymerization kinetics were incorporated in this model. The model was, however, not able to simulate the condensed mode of operation of a polyolefin FBR. In this study, we

Correspondence to: V. V. Ranade. (vv.ranade@ncl.res.in).
Contract grant sponsor: Department of Science and Technology, government of India.

extended PoRE and the underlying mathematical models to incorporate liquid injection and evaporation in polyolefin FBRs.

Although there are several patents on the condensed mode of operation of polyolefin FBRs (see, e.g., refs. 8–11 and references cited therein), the information on the influence of liquid injection on flow, heat transfer, and mixing in FBRs in the open literature is relatively scanty. Werther and Bruhns[12] presented a phenomenological model to describe the injection of liquid in FBRs, whereas Ariyapadi et al.[13] presented a method to measure the horizontal liquid jet penetration in a fluidized bed. Apart from the influence on the hydrodynamics of fluidized beds, the most crucial aspect of successful implementation of the condensed mode of operation is the ensuring of the appropriate distribution and evaporation of injected liquid (droplets). Unfortunately, little information is available about the heat transfer and evaporation of liquid droplets interacting with hot gas–solid mixtures. We critically examine this available information in the following section to estimate the key timescales of evaporation of liquid droplets injected in dense fluidized beds. This information is then used to extend our mathematical model[7] to the condensed mode of operation. The model equations and solution method are discussed in the Mathematical Model section. The mathematical model is then used to determine key issues related to the condensed mode of operation of PP FBRs. The predicted characteristics of the condensed mode of operation and its influence on reactor performance is compared and analyzed. The key findings of this study are highlighted at the end of the article.

DROPLET VAPORIZATION

The interaction of injected liquid droplets and polymer particles govern the fluidization dynamics inside the reactor. Depending on the temperature of the solids and the Leidenfrost temperature of the liquid (the temperature at which droplet levitation occurs), different regimes of heat transfer and evaporation may occur. Therefore, it is necessary to quantify the droplet vaporization length and timescales for a realistic model. Traditionally, the Ranz and Marshall[14] correlation is used to estimate heat transfer between the suspended droplet and surrounding gas. The presence of suspended solid particles in a gas is expected to influence heat transfer from the liquid droplet. Unfortunately, adequate information about this is not available.

Several investigators have studied the heat transfer and evaporation of falling liquid droplets on a hot solid surface.[15–18] Computational fluid dynamics based models have been proposed[17] to explain the droplet dynamics. These models can be used to understand the interactions between the suspended solid particle and the gas. However, at this point, the physics remains poorly understood.

Buchanan[19] analyzed the model of the heating and vaporization of a feed droplet on the basis of the following hypotheses: direct contact, convective heat transfer, and radiative heat transfer. The model based on the direct contact hypothesis can be used to estimate the enhanced heat transfer coefficient by the assumption of infinitely fast heat transfer during droplet/particle collisions. This means that solid particles colliding with the drop leave the drop after they attain thermal equilibrium. This model predicts order of magnitude faster evaporation rates. Buchanan presented an effective heat transfer coefficient (h^*) for vaporizing droplet as follows:

$$h^* = \frac{0.66kRe^{0.25}Pr^{0.333}}{2.35d_p} = \frac{0.66k}{2.35}\left(\frac{\rho_f \upsilon}{\mu}\right)^{0.5} Pr^{0.333} d_p^{-0.5} \quad (1)$$

where k is the thermal conductivity (cal/cm^2 K/s), Re is the Reynolds number, Pr is the Prandtl number, d_p is the average polymer particle diameter (cm), ρ_f is the density of the fluid (g/cm^3), υ is the slip velocity (cm/s), and μ is the viscosity of the fluid (g cm^{-1} s^{-1}). Recently, Nayak et al.[20] developed a mathematical model to simulate the evaporation of liquid droplets injected in gas–solid risers. Their model is suitable for the interaction of large liquid drops with much smaller solid particles. h^* based on their model is estimated as follows:

$$h^* = \frac{\lambda\phi U_{\text{slip}} - D\varepsilon_s\rho_\infty}{4(T_s - T_D)}\left(1 + \left(\frac{D_s}{D_D}\right)\right)^2 \quad (2)$$

where λ is the latent heat (cal/g), ϕ is the activity factor, ρ_∞ is the gas phase density (g/cm^3), U_{slip} is the slip velocity (cm/s), D is the reactor diameter (cm), ε_s is the solid volume fraction, D_s is the solid diameter (cm), T_s is the solid temperature (K), T_D is the droplet temperature (K), and D_D is the droplet diameter (cm). In the case of PP FBRs, injected liquid droplets (atomized when they are injected in the range of ~30–100 μm) are usually much smaller than the PP particles (~700–800 μm). In this case, the consideration of a limiting case of the evaporation of a liquid droplet interacting with a flat hot solid surface is more appropriate.

For the condensed mode of operation of a PP FBR, the temperature of solids is in the range 310–380 K, whereas the temperature of injected propylene is in the range 310–320 K. This available information was used to estimate the evaporation timescale of injected liquid droplets. Preliminary simulations were carried out to determine the time required for

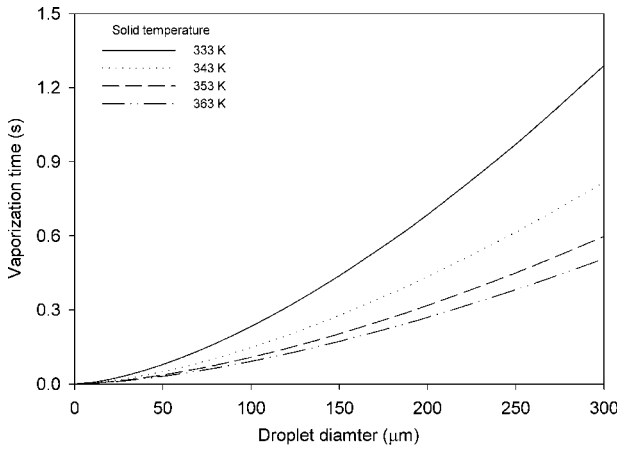

Figure 1 Droplet vaporization times for propylene droplets at 310 K.

the heat up and vaporization of liquid droplets for various initial droplet sizes according to the approach outlined by Buchanan.[19] Figure 1 shows the evaporation times for droplets of different diameters at various solid temperatures. The simulations were carried out for a droplet inlet temperature of 310 K. The time required for complete vaporization of liquid droplets with PP FBR operating conditions was very small [0.023–0.438 s for droplet sizes of 10–150 μm (the typical size of atomized droplets)]. One however, needs to compare these times with the average residence times of gas in the fluidized bed.

While using a mixing cells framework to model a FBR, one can adjust the number of mixing cells to adjust the degree of mixing in the reactor. Wu and Baeyens[21] introduced a mixing index (M) to quantify the extent of mixing in FBRs. M is defined as

$$M = 1 - 0.0067 d_R^{133} \left[2.27 A_r^{-0.21} (U - U_{mf})\right]^{-0.75} \quad (3)$$

where d_R is the particle diameter ratio, A_r is the Archimedes number, U is the gas velocity (cm/s), and U_{mf} is the minimum fluidization gas velocity (cm/s). For a typical polyolefin reactor, the mixing index is in the range 0.4–0.5. This degree of mixing can be adequately captured with three mixing cells.[6] Typically, the minimum fluidization velocities for PP particles (average particle size $\sim$ 700–800 μm) are in the range 0.08–0.1 m/s, and the reactors are usually operated at superficial gas velocities of 4–8U_{mf}. For these ranges, the bubble rise velocities (U_b's) calculated by $U_b = U - U_{mf} + 0.711\sqrt{g d_b}$ [where g is the gravitational acceleration (cm/s^2) and d_b is the bubble diameter (cm)] are on the order of 0.7–1.4 m/s. Thus, for a typical bed height of about 6 m, if we model the bed with three emulsion-phase mixing cells, the minimum gas residence time in a cell would be greater than 1.4 s. This value is much greater than the maximum evaporation time of 0.438 s. Thus, one can assume that the liquid injected in a particular cell is vaporized in that cell itself. In other words, the convection of injected liquid within the reactor may be neglected.

MATHEMATICAL MODEL

A generalized mathematical model with dynamic mass and energy balance coupled PSD was used. The model divides FBR into two phases, namely, the emulsion and bubble phases. The bubble and emulsion phases were modeled as two interacting sets of battery of mixing cells. These two sets of mixing cells were connected via interphase heat and mass transfer. The number of mixing cells in both the emulsion phase and bubble phase could be specified separately (with certain constraints) to achieve the desired degree of mixing in each phase. In addition to these assumptions, we[7] made the following assumptions for liquid injection in developing the mathematical model:

1. Pseudo steady state was assumed for the liquid phase. Because the evaporation time for the liquid was much smaller than typical residence time in a cell, the liquid evaporation dynamics were neglected.
2. Liquid injected in a particular cell evaporated in that cell only (no carryover of liquid to the next cells)
3. The gas produced due to the vaporization of liquid flowed as the bubble phase.
4. The heat required for vaporization was taken from the emulsion phase.
5. The liquid injection process had negligible effect on the hydrodynamic state of the fluidized bed. Local fluidization characteristics were affected due to liquid injection. The characteristics of the bed depended on the amount of liquid injected. In extreme cases, defluidization could occur. As mentioned earlier, information on this aspect is scarce. To realistically account for all of these effects, one would need a detailed hydrodynamic model. Also, in this case, the amount of liquid injected was very small ($\sim$4 wt %). Therefore, we assumed a negligible impact of liquid injection on the state of fluidization. We accounted for the changes in the hydrodynamic parameters (e.g., voidage, bubble diameter) due to the increased volumetric flow rate.

Polymerization kinetics

To describe the kinetic scheme of a heterogeneous Ziegler–Natta catalyst, single and multiple catalyst

active site models have been proposed in the literature.[22–24] The overall scheme is composed of elementary reactions grouped into site activation, propagation, site deactivation, chain transformation, and chain transfer. Hutchinson et al.[24] gave a comprehensive list of reactions in each group. This scheme has been adopted by many researchers.[4,25,26] This scheme was also incorporated in this framework. To facilitate model development, each of the groups was represented by a lumped pseudokinetic rate constant. For details of the kinetic scheme and definitions of the pseudokinetic rate constants, please see the article by Hutchinson et al.[24]

Dynamic reactor model

With the assumptions mentioned previously, dynamic species and energy conservation equations for both the emulsion and bubble phases were written. The dynamic mass and energy balance equations were coupled with steady-state particle population balance equations. The dynamic equations for emulsion-phase energy balance and bubble-phase mass balance are discussed next. All other equations are given in the Appendix. See our earlier article[7] for a detailed explanation of these equations.

Bubble-phase gas species mass balance

The mass balance for the jth gas-phase species in the nth bubble-phase cell is given by eq. (4). The balance includes the amount of species j entering the bubble cell from the $(n-1)$th cell, the amount of species j leaving the nth bubble cell, the mass transfer from the corresponding emulsion cell, and the amount generated due to the vaporization of liquid in that particular cell:

$$\frac{d\left(C^n_{j,B}\right)}{dt} = \frac{1}{V^n_b}\left\{a^{n-1}_B u^{n-1}_{g,B} C^{n-1}_{j,B} - a^n_B u^n_{g,B} C^n_{j,B}\right\} - k^{i,n}_{be}\left\{C^n_{j,B} - C^i_{j,E}\right\} + \frac{q^i_{\text{gas,vapor}}\rho_{\text{gas}} fr_j}{MW_j} \quad (4)$$

where u is the velocity (cm/s), C is the concentration of the monomer (mol/cm^3), the subscripts b and B refer to the bubble phase, V is the volume (cm^3), a is the cross-sectional area (cm^2), the subscript g and ''gas'' refer to the gas, the subscripts e and E refer to the emulsion phase, q is the mass flow rate (g/s), the superscript i refers to a specific emulsion cell, the subscript ''vapor'' refers to the vapor, ρ is the polymer density (g/cm^3), fr is the species mass fraction in liquid, and MW is the molecular weight (g/mol). The velocity of gas rising up from the nth bubble cell is set equal to the bubble rise velocity of bubble in the nth cell. It is assumed that no reaction takes place in the bubble phase.

Emulsion-phase energy balance

The energy balance for the ith emulsion cell compartment is given by eq. (5). We accounted for the additional terms arising from the vaporization of the liquid [last term in eq. (5)]:

$$\begin{aligned}\frac{dT^i_e}{dt} = {} & \frac{1}{V^i_e\left(\sum_{j=1}^{N_{\text{monomer}}} \varepsilon_{mf} C^i_{j,E} M_j C_{p_{\text{g},j}} + (1-\varepsilon_{mf}) C_{p_{\text{poly}}} \rho^i_{\text{mix}}\right)} \\ & \times \left\{ a^{i-1}_E u^{i-1}_{g_{\text{up}},E} \sum_{j=1}^{N_{\text{monomer}}} C_{p_{\text{g},j}} C^{i-1}_{j,E} M_j \left(T^{i-1}_e - T_{\text{ref}}\right) \right. \\ & + a^{i+1}_E u^{i+1}_{g_d,E} \sum_{j=1}^{N_{\text{monomer}}} C_{p_{\text{g},j}} C^{i+1}_{j,E} M_j \left(T^{i+1}_e - T_{\text{ref}}\right) \\ & + q^i_{s,\text{in}} C_{p_{\text{in}}} \left(T_{\text{in}} - T_{\text{ref}}\right) - a^i_E \left(u^i_{g_{\text{up}},E} + u^i_{g_d,E}\right) \\ & \times \sum_{j=1}^{N_{\text{monomer}}} C_{p_{\text{g},j}} C^i_{j,E} M_j \left(T^i_e - T_{\text{ref}}\right) \\ & + q^{i-1}_{s,\text{up}} C_{p_{\text{poly}}} \left(T^{i-1}_e - T_{\text{ref}}\right) + q^{i+1}_{s,d} C_{p_{\text{poly}}} \left(T^{i+1}_e - T_{\text{ref}}\right) \\ & - \left(q^i_{s,d} + q^i_{s,\text{up}} + q^i_{s,\text{out}}\right) C_{p_{\text{poly}}} \left(T^i_e - T_{\text{ref}}\right) \\ & + \sum_{j=1}^{N_{\text{monomer}}} V^i_e (1-\varepsilon_{mf}) R^i_{C^i_j,E} M w_j \Delta H_{r_j} \\ & \left. - \sum_{n=1}^{N_{\text{BEratio}}} h^{i,n}_{be} V^n_b \left(T^i_e - T^n_b\right) \right\} - H^i_{\text{vapor}} \end{aligned} \quad (5)$$

where T is the temperature (K), N_{monomer} is the number of monomers, ε_{mf} is the minimum fluidation voidage, the subscript ''ref'' refers to the reference, the subscript d refers to downflow, the subscript s refers to the solids, the subscript ''in'' means ''in,'' the subscript ''up'' refers to upflow, the subscript ''poly'' refers to the polymer, the subscript ''mix'' refers to the bulk, R is the rate of reaction of the species (mol/cm^3/s), N_{BEratio} is the ratio of the number of bubble cells to emulsion cells, h_{be} is the heat transfer coefficient between the bubble and emulsion phases (cal/cm^3/s), and H is the heat of vaporization (cal/g).

Changes in the hydrodynamic parameters

Liquid injection leads to a change in the volumetric flow rate of gas going out of each cell. Ultimately, this changes the overall hydrodynamics (bed voidage, bubble size, emulsion-phase velocity, bubble

velocity, etc.) in the bed and, hence, affects the performance of the reactor. To account for the changes in the hydrodynamic parameters, the following equations were coupled with the dynamic mass and energy balance equations.

Amount of liquid injected in emulsion cell i.

$$q^i_{\text{liq}} = \frac{X_{\text{liq}} q_{\text{gas,in}} \rho_{\text{gas}}}{(1 - X_{\text{liq}}) \rho_{\text{liq}} N_{\text{etanks}}} \tag{6}$$

X_{liq} is the mass fraction of liquid.

Amount of vapor produced due to the vaporization of liquids.

$$q^i_{\text{gas,vapour}} = \sum_{j=1}^{N_{\text{monomer}}} \frac{q^i_{\text{liq}} \rho_{\text{gas},j} fr_j}{MW_j \frac{P}{RT^i_e}} \tag{7}$$

P is pressure (N/m^2).

Total volumetric flow rate of gas going out of cell i.

$$q^i_{\text{gas},t} = q^i_{\text{gas,B}} + q^{i,N_{\text{monomer}}}_{\text{gas},B} \tag{8}$$

t denotes total.

The total volumetric gas flow rate coming into the reactor can be calculated as follows:

$$q_{\text{gas},in} = \alpha u_g \tag{9}$$

The total volumetric gas flow rate going out of the reactor is calculated as follows:

$$\begin{aligned} &\text{For} \quad n = N_{\text{BEratio}} \\ &q^i_{\text{gas,out}} = q^{\text{n}}_{\text{gas},E} + q^n_{\text{gas},B} \end{aligned} \tag{10}$$

Amount of gas coming into emulsion cell i.

$$q^i_{\text{gas},E} = \varepsilon_{\text{mf bed}}\, u_{mf} + \sum_{n=1}^{n} q^{i,n}_{\text{gas},B} \tag{11}$$

Amount of gas coming into bubble cell n.

$$\begin{aligned} &\text{For } n = 1 \quad q^n_{\text{gas},B} = q^{i-1}_{\text{gas},t} - a_{\text{bed}} u_{mf} - q^{i,n}_{\text{gas},tfr} + q^{i-1}_{\text{gas,vapor}} \\ &\text{For } n \neq 1 \quad q^n_{\text{gas},B} = q^{n-1}_{\text{gas},t} - q^{i,n}_{\text{gas},trf} \end{aligned} \tag{12}$$

These equations were used to calculate the hydrodynamic parameters (bed voidage, bubble size, emulsion-phase velocity, bubble velocity, etc.).

The amount of heat required to convert the liquid monomer into gas is equal to the latent heat of vaporization of the liquid, which was calculated as

$$H^i{}_{\text{vapor}} = \sum_{j=1}^{N_{\text{monomer}}} q^i{}_{\text{liq},j} \rho_{\text{liq},j} \lambda_{\text{liq},j} \tag{13}$$

Steady-state particle population balance

The estimation of average particle size in the reactor is crucial for the accurate prediction of PP FBR performance. To calculate the average particle size in a reactor, the steady-state particle population balance model was incorporated into the model. The steady-state population balance equations were written for each of the emulsion mixing cells. The direct integration approach to population balance equations[27] was followed for the derivation of the particle population balance equations.

The steady-state particle population balance equations can be written as follows. For the bottom compartment ($i = 1$)

$$\frac{dw^i_r}{dr} = q^i_{s,in} X^i_{\text{cat},in} p^i_{Or} + \frac{q^{i+1}_{s,d} w^{i+1}_r}{W^{i+1}_{\text{bed}} R^{i+1}_r} + \frac{K_r w^{N_{\text{etanks}}}_r}{R^{N_{\text{etanks}}}_r} - \frac{\left(q^i_{s,\text{out}} + q^i_{s,up}\right) w^i_r}{W^i_{\text{bed}} R^i_r} + \frac{3w^i_r}{r} \tag{14}$$

where O refers to the catalyst, w^i_r is a dummy variable ($= W^i_{bed} p^i_{1r} R_r$), where the subscript 1 refers to the product or bed; r is the radius of the particle (cm); the subscript ''cat'' refers to the catalyst; p is the particle density function (cm^{-1}); W is the weight (g); R_r is the rate of increase of the radius for a particle of radius r (cm/s); and K_r is an elutriation constant (s^{-1}). For the ith tank, $i > 1$ and $i < n_e$

$$\frac{dw^i_r}{dr} = q^i_{s,in} X^i_{\text{cat},in} p^i_{\text{or}} + \frac{q^{i+1}_{s,d} w^{i+1}_r}{W^{i+1}_{\text{bed}} R^{i+1}_r} + \frac{q^{i-1}_{s,up} w^{i-1}_r}{W^{i-1}_{\text{bed}} R^{i-1}_r} - \frac{\left(q^i_{s,\text{out}} + q^i_{s,up} + q^i_{s,d}\right) w^i_r}{W^i_{\text{bed}} R^i_r} + \frac{3w^i_r}{r} \tag{15}$$

For the top compartment ($i = N_{\text{etanks}}$)

$$\frac{dw^i{}_r}{dr} = q^i_{s,in} X^i_{\text{cat},in} p^i_{or} + \frac{q^{i-1}_{s,d} w^{i+1}_r}{W^{i-1}{}_{\text{bed}} R^{i-1}{}_r} - \frac{K_r w^{NE}_r}{R^{NE}{}_r} - \frac{\left(q^i_{s,\text{out}} + q^i_{s,d}\right)}{W^{i-1}{}_{\text{bed}} R^{i-1}{}_r} + \frac{3w^i_r}{r} \tag{16}$$

where the subscript 0 refers to the initial time or the catalyst. K_r is given by

$$K_r = \frac{k^* a_E^{N_{\text{etanks}}}}{W^{N_{\text{etanks}}}_{\text{bed}}} \tag{17}$$

where $k^*$is an elutriation constant ($g/cm^2/s$). $R^i{}_r$ is given by

$$R^i_r = \frac{dr}{dt} = \frac{4R^i_{\text{poly}} d^3_{\text{cat}}}{3\rho_{\text{mix}} r^2} \tag{18}$$

d is Diameter (cm).

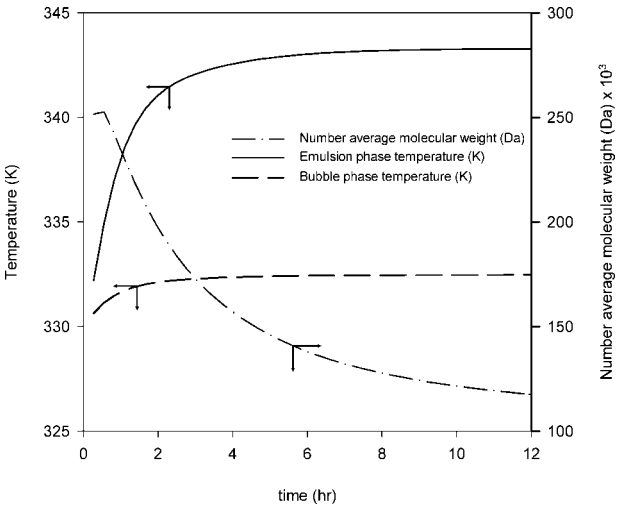

Figure 2 Typical dynamical output.

These modified equations were implemented in the PoRE framework. To solve the differential, the ODEPACK library from Los Alamos National Laboratory (LANL)[28] was used. The solution methodology and numerical issues associated with the solving coupled reactor model and population balance model were discussed in our earlier article.[7]

RESULTS AND DISCUSSION

The developed model was used to simulate the performance of a FBR for propylene homopolymerization operated in the condensed mode. A two-site kinetic scheme was used. The kinetic data as given by Zacca et al.[25] were used for the simulations. We assumed that catalyst was fully activated at time $t = 0$. The simulation parameters we used were given in our earlier article.[7] The simulations were carried out to evaluate the effect of the main operating parameters (amount of liquid injected, gas feed temperature, and catalyst feed rate) on the performance of the reactor. The number of emulsion cells was fixed at three.[6] In most cases, it was reasonable to approximate the bubble phase to be in plug flow. We observed that increasing the bubble cells beyond nine did not have any significant effect on the output. Therefore, three emulsion cells and 3×3 bubble cells were used in further simulations. Dynamic simulations were carried out for changes in various operating parameters until the steady state was reached. These steady-state values were used subsequently to determine the effect of the parameters. Figure 2 shows the typical results of a dynamical simulation. Preliminary numerical experiments were carried out to determine the tolerances and model-adjustable parameters. Because it is extremely hard to get industrial data on olefin polymerization systems for model validation, the model was also tested against the simulation results of Zacca et al.[25] This comparison was reported in our previous article.[7]

Effect of the operating variables

Figure 3 shows the effect of the catalyst feed rate and liquid injection ratio on the emulsion-phase temperature. For any given liquid injection rate, the emulsion-phase temperature increased exponentially with catalyst feed rate. For higher catalyst feed rates, the reaction rate increased, and the safe operating region narrowed down and vice versa. With the addition of liquid, additional heat could be withdrawn from the reactor; thus, for the same catalyst feed rates, lower emulsion-phase temperatures were possible. In other words, the addition of liquid widened the safe operational window. For no liquid addition, the emulsion-phase temperature reached a maximum operating temperature (353 K) at a catalyst feed rate of 0.28 g/s. Even a 1 wt % addition of liquid significantly widened the operational window (catalyst feed rate = 0.325 g/s).

Because a coupled model was used in this study, the average polymer particle size for a given set of operating conditions and kinetics could be predicted with the model. Figure 4 shows the effect of the operating conditions (catalyst feed rate and amount of liquid added) on the average polymer particle size present in the reactor. As the catalyst flow rate was increased, the average particle size increased due to the increased rate of polymerization. Similar to the effect on emulsion temperature, for the same catalyst feed rate, the average particle size decreased with increasing amount of liquid added to the reactor. As shown in Figure 4, the wide particle size variation caused changes in the hydrodynamic parame-

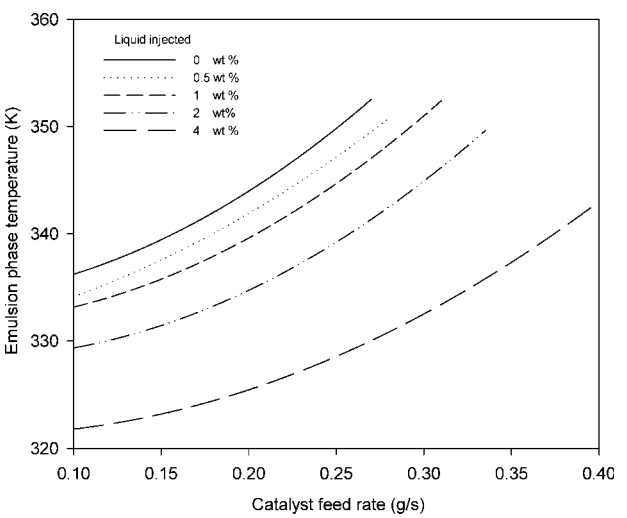

Figure 3 Effect of the catalyst feed rate and liquid injection on the emulsion temperature.

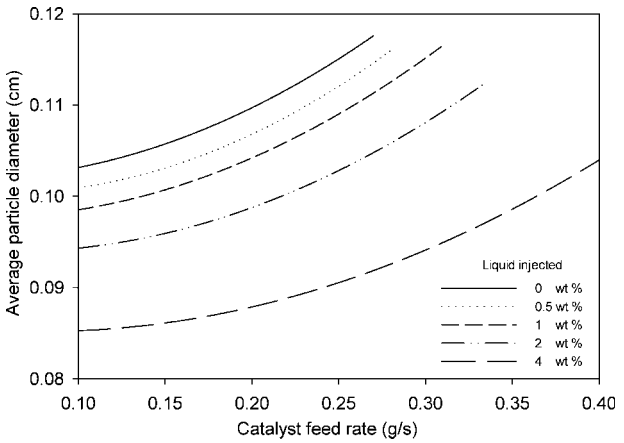

Figure 4 Effect of the catalyst feed rate and liquid injection on the average particle diameter.

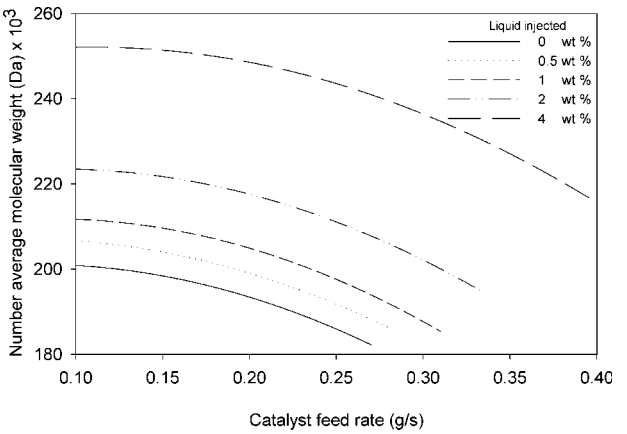

Figure 6 Effect of the catalyst feed rate and liquid injection on NAMW.

ters, and hence, the model predictions were considerably different than those of uncoupled models. However, for a given emulsion-phase temperature, only a 2–5% change in the average particle size (regardless of catalyst feed rate or liquid injection rate) was observed (see Fig. 5). The difference in average particle size at different liquid injection rates narrowed at higher temperatures.

The effect of the operating conditions on the number-average molecular weight (NAMW) is shown in Figure 6. NAMW decreased with catalyst feed rate as increasing the catalyst feed rate increased the polymer production and decreased the solid residence time in the reactor. As the amount of liquid injected in the reactor was increased, for the same catalyst feed rate, lower temperatures were encountered. This reduced the polymer production and increased the solid residence time. Therefore, a polymer with a higher NAMW was obtained. Similar results were obtained for the weight-average molecular weight and polydispersity index (PDI). Furthermore, for the operating conditions examined, PDI varied between 4.4 and 5.2 (see Fig. 7). Such results are useful in the quantification of the operating window.

Capacity increase in the condensed mode of operations

Figure 8 shows the effective reactor and catalyst utilization for the same reactor hardware due to liquid injection. Through the injection of monomer liquid reactor hardware, the amount of polymer produced per unit volume of the reactor increased substantially. The capacity increased up to 85% when the weight percentage of monomer liquid in the feed stream was increased from 0 (normal mode) to 4%. To evaluate this, for any given liquid ratio in the

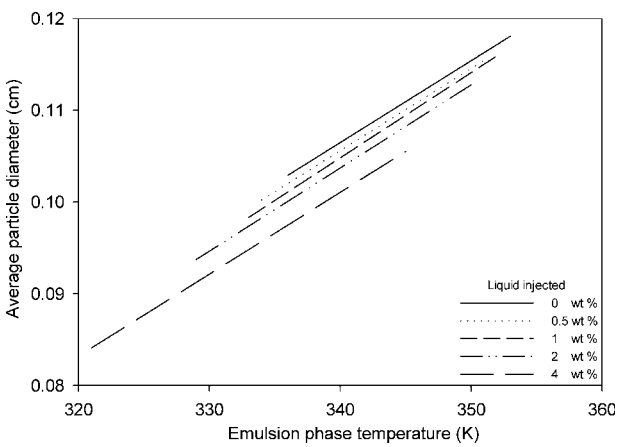

Figure 5 Effect of the emulsion-phase temperature on the average particle diameter.

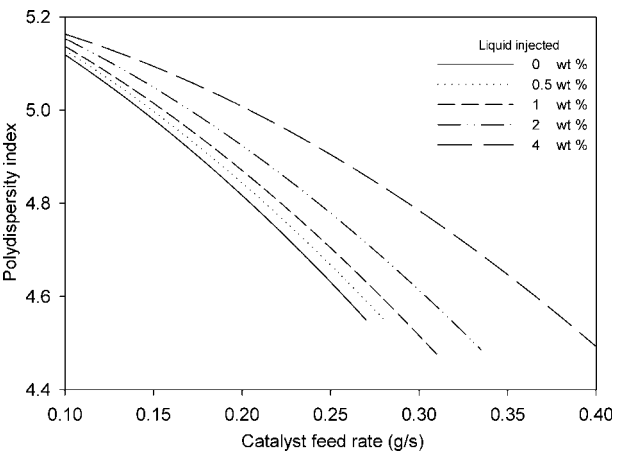

Figure 7 Effect of the catalyst feed rate and liquid injection on PDI.

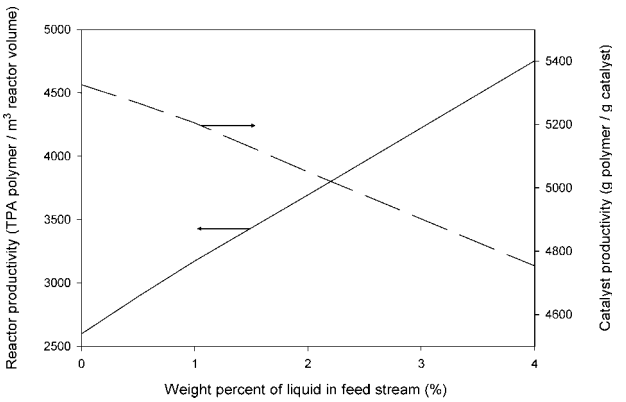

Figure 8 Increase in productivity due to liquid injection.

feed, the catalyst feed rate was adjusted such that an emulsion temperature of 345 K was achieved. The polymer production rate at this point was used to calculate the increase in capacity over the normal mode operations. The capacity increased almost linearly with the weight percentage of liquid added to the feed stream. This was because with the addition of liquid, to achieve the same temperature, the reactor could push through more catalyst and, thus, increase the production rate. On the secondary axis of Figure 8, the polymer produced per gram of catalyst (catalyst utilization) is plotted against the amount of liquid injected. As shown, a lower amount of polymer was produced per gram of catalyst as the liquid weight fraction entering the reactor increased. The catalyst utilization decreased from 5325 g of polymer/g of catalyst to 4753 g of polymer/g of catalyst with increasing liquid weight fraction from 0 to 4%. This means that one needed to push 25% more catalyst through the reactor than the anticipated increase in production. Thus, one could control the production rate by conveniently controlling the catalyst feed rate.[9] Better heat removal capacity due to the injected liquid was also found to widen the safe operating window for the given reactor hardware (see Figs. 4 and 5).

The condensed mode of operation of the PP fluidized bed looked promising. The model presented in this article enabled us to access the reactor performance for different operating and design parameters. However, the model requires a realistic description of the underlying hydrodynamics for useful predictions. Even though the liquid evaporation timescales are quite small, the addition of liquid influences the local fluidization behavior of the bed. Therefore, the presence of liquid around the fluidizing particles on bridging, agglomeration and possible defluidization needs to be studied more extensively. Experiments and detailed computational fluid dynamic models need to be developed to determine possible local defluidization and its impact on heat transfer. The atomization of liquid injected in fluidized beds also need to be investigated further. The impact of small liquid droplets on hot solids and subsequent heat transfer and evaporation needs to be studied further. Some of these aspects are being studied in our group. The results of such studies on the interaction of evaporating liquid droplets and fluidized particles in combination with the model presented here will provide a useful basis for designing and operating the condensed mode of PP FBRs.

CONCLUSIONS

A model for the condensed mode of operation of PP reactors was developed. Key time and length scales in the evaporation of liquid droplets in the presence of solids were evaluated in the development of the model. The developed model was incorporated in the PoRE simulator that we[7] described. This was then used to compare the performance of a PP FBR for normal and condensed modes of operation. The model was also used to determine the effects of catalyst feed, product removal, and liquid addition on the overall performance of the reactor. The key findings of this work may be summarized as follows:

1. The time scales of the evaporation of liquid droplets in the range of 10–150 μm were estimated to be within 0.023–0.438 s.
2. A quasisteady approximation for evaporating liquid appeared to be applicable.
3. The injection of liquid into the PP FBR widened the safe operating window.
4. A considerable increase in the capacity (kg of polymer/m^3 of reactor) was achieved with liquid injection. For a liquid addition of 4%, the reactor capacity increased by 85%.
5. The productivity of catalyst (kg of polymer/kg of catalyst), however, decreased with liquid injection. For a liquid addition of 4%, the catalyst productivity decreased by 25%.

The model developed in this study can be used to design and optimize PP reactors. Further research on the influence of injected liquid on the hydrodynamics of bubbling fluidized beds is needed to complement the model and the results discussed here.

One of the authors (R.P.U.) thanks the Council of Scientific and Industrial Research for providing a research fellowship.

APPENDIX

Dynamic reactor model equations

Catalyst mass balance

For the ith emulsion cell, the catalyst mass balance in the cell is

$$\frac{dX^i_{\text{cat}}}{dt} = \frac{\left\{\begin{array}{c} q^i_{s,\text{in}}X^i_{\text{cat,in}} + q^{i-1}_{s,\text{up}}X^{i-1}_{\text{cat}} + q^{i+1}_{s,\text{up}}X^{i+1}_{\text{cat}} \\ -\left(q^i_{s,\text{out}} + q^i_{s,\text{up}} + q^i_{s,d}\right)X^i_{\text{cat}} \end{array}\right\}}{V^i_e(1-\varepsilon_{mf})\left(2X^i_{\text{cat}}(\rho_{\text{cat}} - \rho_{\text{poly}}) + \rho_{\text{poly}}\right)} \quad \text{(A1)}$$

Mass balance for species S

Species balances for potential active sites, vacant sites, deactivated sites, live polymer moments, and bulk polymer moments were written for each emulsion cell. The overall mass balance for any species S at the kth site in the ith emulsion cell is given by

$$\frac{dS^i_k}{dt} = \frac{1}{V^i_e(1+\varepsilon_{mf})}\left\{\frac{q^i_{s,\text{in}}X^i_{\text{cat,in}}S^i_{k,\text{in}}}{\rho_{\text{cat}}} + \frac{q^{i-1}_{s,\text{up}}S^{i-1}_k}{\rho^{i-1}_{\text{mix}}} + \frac{q^{i+1}_{s,d}S^{i+1}_k}{\rho^{i+1}_{\text{mix}}} - \frac{\left(q^i_{s,\text{out}} + q^i_{s,\text{up}} + q^i_{s,d}\right)S^i_k}{\rho^i_{\text{mix}}}\right\} + R^i_{S_k} \quad \text{(A2)}$$

where S is the concentration of species S (mol/cm^3).

Emulsion-phase gas species mass balance

The generalized balance equation for the jth gas-phase species (n monomers and hydrogen) in the ith emulsion cell follows:

$$\frac{dC^i_{j,E}}{dt} = \frac{1}{V^i_e\varepsilon_{mf}}\left\{\begin{array}{l} a^{i-1}_E u^i_{g_{\text{up}}E}C^{i-1}_{j,E} + a^{i+1}_E u^{i+1}_{g_d,E}C^{i+1}_{j,E} \\ - a^i_E C^i_{j,E}\left(u^i_{g_{\text{up}},E} + u^i_{g_dE}\right) - q^i_{s,d}\rho^i_{\text{mix}}C^i_{j,E} \\ + q^{i+1}_{s,d}\rho^{i+1}_{\text{mix}}C^{i+1}_{j,E} + q^{i-1}_{s,\text{up}}\rho^{i-1}_{\text{mix}}C^{i-1}_{j,E} \end{array}\right\} - \frac{R^i_{C^i_{j,E}}(1-\varepsilon_{mf})}{\varepsilon_{mf}} + \frac{\sum_{n=1}^{N_{\text{BEratio}}} k^{i,n}_{be}V^n_b\left\{C^n_{j,B} - C^i_{j,E}\right\}}{V^i_e\varepsilon_{mf}} \quad \text{(A3)}$$

where k_{be} is the mass transfer coefficient between the bubble and emulsion phases (s^{-1})

Bubble-phase energy balance

The energy balance for nth bubble cell is given by

$$\frac{dT^n_b}{dt} = \frac{1}{V^n_b\sum_{j=1}^{N_{\text{monomer}}} C_{pg_j}Mw_jC^n_{j,B}} \times\left\{a^{n-1}_B u^{n-1}_{g,B}\sum_{j=1}^{N_{\text{monomer}}} C_{pg_j}Mw_jC^{n-1}_{j,B}\left(T^{n-1}_b - T_{\text{ref}}\right) - a^n_B u^n_{g,B}\sum_{j=1}^{N_{\text{monomer}}} C_{pg_j}Mw_jC^n_{j,B}\left(T^n_b - T_{\text{ref}}\right)\right\} + \frac{h^{i,n}_{be}\left(T^i_e - T^n_b\right)}{\sum_{j=1}^{N_{monomer}} C_{pg_j}Mw_jC^n_{j,B}} \quad \text{(A4)}$$

NOMENCLATURE

a	Cross-sectional area (cm^2)
A_r	Archimedes number
C	Concentration of monomer (mol/cm^3)
C_p	Specific heat (cal g^{-1} K^{-1})
D	Reactor diameter (cm)
D_g	Diffusivity of the gas (cm^2/s)
D_s	Solid diameter (cm)
D_D	Droplet diameter (cm)
d_b	Bubble diameter (cm)
d_p	Average polymer particle diameter (cm)
f_r	Species mass fraction in liquid
g	Gravitational acceleration (cm/s^2)
H	Heat of vaporization (cal/g)
h^*	Effective heat transfer coefficient (cal/cm^3/s)
h_{be}	Heat transfer coefficient between the bubble and emulsion phases (cal/cm^3/s)
k	Thermal conductivity (cal/cm^2 K/s)
k^*	Elutriation constant (g/cm^2/s)
k_{be}	Mass transfer coefficient between the bubble and emulsion phases (s^{-1})
K_r	Elutriation constant (s^{-1})
M	Mixing index
MW	Molecular weight (g/mol)
N_{BEratio}	Ratio of the number of bubble cells to emulsion cells
N_{etanks}	Number of emulsion cells
p	Particle density function (cm^{-1})
Pr	Prandtl number
q	Mass flow rate (g/s)
r	Radius of particle (cm)
R	Rate of reaction of species (mol/cm^3/s)
Re	Reynolds number
R_r	Rate of increase of radius for a particle of radius r (cm/s)
S	Concentration of species S (mol/cm^3)

T	Temperature (K)
T_s	Solid temperature (K)
T_D	Droplet temperature (K)
U	Gas velocity (cm/s)
U_{slip}	Slip velocity (cm/s)
V	Volume (cm^3)
W	Weight (g)
X_{cat}	Catalyst weight fraction (g of catalyst/g of solid)
X_{Ti}	Weight fraction of Ti in the catalyst
δ	Bubble fraction
ε_{mf}	Minimum fluidization voidage
ε_s	Solid volume fraction
λ	Latent heat (cal/g)
μ	Viscosity of the fluid (g cm^{-1} s^{-1})
ϕ_s	Sphericity of the polymer particle
ρ	Polymer density (g/cm^3)
ρ_f	Density of the fluid (g/cm^3)

Subscripts

b, B	Bubble phase
cat	Catalyst
d	Downflow
e, E	Emulsion phase
g	Gas
in	In
j	*j*th monomer
k	*k*th active site
max	Maximum
mf	Minimum fluidization
mix	Bulk
poly	Polymer
r	Radius *r*
ref	Reference
s	Solids
up	Upflow
v	Vapor
0	Initial or catalyst
1	Product or bed
2, elut	Elutriation

Superscripts

i	*i*th emulsion cell
n	*n*th bubble cell

References

1. Hatzantonis, H.; Kiparissides, C. Chem Eng Sci 1998, 53, 3251.
2. Sinclair, Kenneth B. ''Third Generation Polyolefin Technologies and Their Capabilities'' SPE Polyolefins IX International Conference Feb. 26, 1995.
3. McAuley, K. B.; Talbot, J. P.; Harris, T. J. Chem Eng Sci 1994, 49, 2035.
4. Fernandes, F. A. N.; Lona, L. M. F. J Appl Polym Sci 2001, 81, 321.
5. Choi, K. Y.; Ray, W. H. Chem Eng Sci 1985, 40, 2261.
6. Alizadeh, M.; Mostoufi, N.; Pormahdian, S.; Soutudeh-Gharebagh, R. Chem Eng J 2004, 97, 27.
7. Harshe, Y. M.; Utikar, R. P.; Ranade, V. V. Chem Eng Sci 2004, 59, 5145.
8. Chinh, J. C.; Fillippelli, M. C. H.; Newton, D.; Power, M. B.U.S. Pat. 5,733,510 (1998).
9. Jenkins, J. M., III; Jones, R. L.; Jones, T. M.; Beret, S.U.S. Pat. 4,588,790 (1986).
10. Olson, R. W.; Howley, T. J.U.S. Pat. 6,815,512 B1 (2004).
11. Olson, R. W.; Howley, T. J.U.S. Pat. 7,025,938 B2 (2006).
12. Werther, J.; Bruhns, S. Int J Chem React Eng 2004, 2, A31.
13. Ariyapadi, S.; Berruti, F.; Briens, C.; McMillan, J.; Zhou, D. Int J Chem React Eng 2004, 2, A22.
14. Ranz, W. E.; Marshall, W. R., Jr. Chem Eng Prog 1952, 48, 141 and 173.
15. Chandra, S.; Di Marzo, M.; Qiao, Y. M.; Tartarini, P. Fire Saf J 1996, 27 (2), 141.
16. Crafton, E. F.; Black, W. Z. Int J Heat Mass Transfer 2004, 47, 1187.
17. Ge, Y. Ph.D. Dissertation, Ohio State University, 2005.
18. Utikar, R. P.; Mehra, A.; Ranade, V. V. Presented at the 6th International Symposium on Catalysis in Multiphase Reactors and the 5th International Symposium on Multifunctional Reactors, Pune, India, January 2007.
19. Buchanan, J. S. Ind Eng Chem Res 1994, 33, 3104.
20. Nayak, S. V.; Joshi, S. L.; Ranade, V. V. Chem Eng Sci 2005, 60, 6049.
21. Wu, S. Y.; Baeyens, J. Powder Technology 1998, 98, 139.
22. Ray, W. H. J Macromol Sci Rev Macromol Chem Phys 1972, 8, 1.
23. McAuley, K. B.; MacGregor, J. F.; Hamilec, A. E. AIChE J 1990, 36, 837.
24. Hutchinson, R. A.; Chen, C. M.; Ray, W. H. J Appl Polym Sci 1992, 44, 1389.
25. Zacca, J. J.; Debling, J. A.; Ray, W. H. Chem Eng Sci 1996, 51, 4859.
26. Hatzantonis, H.; Yiannoulakis, H.; Yiagopoulos, A.; Kiparissides, C. Chem Eng Sci 2000, 55, 3237.
27. Selçuk, N.; Oymak, O.; Degirmrnci, E. Powder Technol 1996, 87, 269.
28. Hindmarsh, A. C. In Scientific Computing; Stepleman, R. S., et al., Eds.; IMACS Transactions on Scientific Computation 1; North-Holland: Amsterdam, 1983; p 55.